Advances in Applied Mathematics and Mechanics
Adv. Appl. Math. Mech., Vol. **2**, No. 5, pp. 545-563

DOI: 10.4208/aamm.10-10S02
October 2010

Lattice Boltzmann Method for Reacting Flows in Porous Media

Qinjun Kang[1,*], Peter C. Lichtner[1] and David R. Janecky[2]

[1] *Computational Earth Sciences Group, Los Alamos National Laboratory, Los Alamos, NM 87545, U.S.A*
[2] *Ecology and Air Quality Group, Los Alamos National Laboratory, Los Alamos, NM 87545, U.S.A*

Received 27 April 2010; Accepted (in revised version) 4 May 2010
Available online 13 July 2010

Abstract. We review recent developments in lattice Boltzmann method for reacting flows in porous media. We present the lattice Boltzmann approaches for incompressible flow, solute transport and chemical reactions in both the pore space and at the fluid/solid interfaces. We discuss in detail the methods to update solid phase when significant mass transfer between solids and fluids is involved due to dissolution and/or precipitation. Applications in different areas are presented and perspectives of applying this method to a few important fields are discussed.

PACS (2006): 47.70.-n, 82.33.Ln, 47.56.+r

Key words: Reactive flows, lattice Boltzmann method, porous media, pore scale.

1 Introduction

Reacting flows in natural and man-made porous media are ubiquitous, particularly in various energy, earth and environment systems. Examples include electrochemical energy conversion devices (fuel cells and batteries), stimulation of petroleum reservoirs, geologic storage of carbon dioxide and nuclear wastes, subsurface contaminant migration, bioremediation etc. In these examples, the inherently complex morphology of such porous media coupled with multi-physicochemical transport and interfacial processes over multiple length scales makes this problem notoriously difficult and consequently poses several open questions. On one hand, most of the key processes, including fluid mobility, chemical transport, adsorption and reaction, are ultimately governed by the pore-scale interfacial phenomena, which occur at scales of microns.

*Corresponding author.
URL: `http://ees.lanl.gov/pflotran/staff/lichtner/lichtner.shtml`
Email: qkang@lanl.gov (Q. J. Kang), lichtner@lanl.gov (P. C. Lichtner), janecky@lanl.gov (D. R. Janecky)

On the other hand, because of the wide disparity in length scales, it is virtually impossible to solve the pore-scale governing equations at the scale of interest. As a result, a continuum formulation (macroscopic approach) of reactive transport in porous media based on spatial averages and empirical parameters is often employed. As the spatial averaging is taken over length scales much larger than typical pore and grain sizes, spatial heterogeneities at smaller scales are unresolved. These unresolved heterogeneities, together with the empirical parameters often unrelated to physical properties, lead to significant uncertainties in reactive flow modeling at the larger scale. Therefore, to reduce uncertainties in the numerical modeling of reactive transport processes at the scale of interest, it is imperative to better understand these processes at the pore scale and to incorporate pore-scale effects in the continuum scale [34,35].

The problem of reacting flows in porous media has been studied extensively at the pore scale using various approaches under different simplifying conditions [2,3, 8,10,12,17,20–23,25–28,43,53]. The lattice Boltzmann method (LBM), a relatively new numerical method in computational fluid dynamics [6,44], has undergone great advances and developed into a powerful numerical tool for simulating complex fluid flows and modeling physics in fluids in the past two decades. Owning to its advantage in handling nonequilibrium dynamics, especially in fluid flow applications involving interfacial dynamics and its ease to treat complex boundaries (geometries), the LBM offers a promising approach for investigating pore-scale phenomena involving reacting flows in porous media. In this article, we review recent developments in LBM for reacting flows in porous media. Earlier work on lattice gas and lattice Boltzmann methods and their applications in reaction-diffusion systems can be found in the excellent review by Chen et al. [5].

2 Lattice Boltzmann method for fluid flow

The flow of a single aqueous fluid phase in the pore space of a porous medium can be simulated by the following evolution equation (the so-called LBGK equation) [4,41]

$$f_\alpha(\mathbf{x}+\mathbf{e}_\alpha\delta t, t+\delta t) = f_\alpha(\mathbf{x},t) - \frac{f_\alpha(\mathbf{x},t) - f_\alpha^{\rm eq}(\mathbf{x},t)}{\tau}. \tag{2.1}$$

In the above equation, δt is the time increment, f_α the distribution function along the α direction in velocity space, $f_\alpha^{\rm eq}$ the corresponding equilibrium distribution function and τ the dimensionless relaxation time. For the commonly used two-dimensional, nine-speed LB model (D2Q9) as shown in Fig. 1, the discrete velocities $\mathbf{e}_\alpha$ have the following form:

$$\mathbf{e}_\alpha = \begin{cases} 0, & \alpha = 0, \\ \left(\cos\frac{(\alpha-1)\pi}{2}, \sin\frac{(\alpha-1)\pi}{2}\right)c, & \alpha = 1-4, \\ \sqrt{2}\left[\cos\left(\frac{(\alpha-5)\pi}{2}+\frac{\pi}{4}\right), \sin\left(\frac{(\alpha-5)\pi}{2}+\frac{\pi}{4}\right)\right]c, & \alpha = 5-8, \end{cases} \tag{2.2}$$

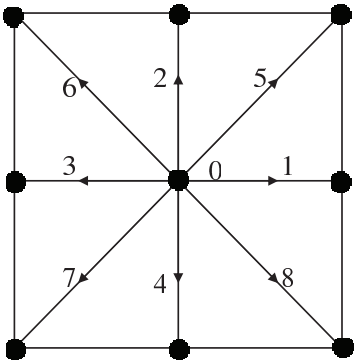

Figure 1: Schematic illustration of a D2Q9 lattice.

and $f_\alpha^{\rm eq}$ is given by

$$f_\alpha^{\rm eq}(\rho,\mathbf{u}) = \omega_\alpha \rho + \rho s_\alpha(\mathbf{u}), \tag{2.3}$$

where

$$s_\alpha(\mathbf{u}) = \omega_\alpha\Big(\frac{3\mathbf{e}_\alpha\cdot\mathbf{u}}{c^2} + \frac{9(\mathbf{e}_\alpha\cdot\mathbf{u})^2}{2c^4} - \frac{3\mathbf{u}\cdot\mathbf{u}}{2c^2}\Big). \tag{2.4}$$

In the above equations,

$$c = \frac{\delta x}{\delta t},$$

where δx is the space increment and ω_α are weight coefficients with ω_0=4/9, ω_α=1/9 for α=1,2,3,4 and ω_α=1/36 for α=5,6,7,8. It has been shown that Eq. (2.1) can be proved to recover the continuity and Navier-Stokes (NS) equations in the nearly incompressible limit [4,41]. The fluid density and velocity are calculated using

$$\rho = \sum_\alpha f_\alpha, \tag{2.5a}$$

$$\rho\mathbf{u} = \sum_\alpha \mathbf{e}_\alpha f_\alpha. \tag{2.5b}$$

The density variation and Mach number of the fluid must be very small for an accurate simulation of incompressible flows. These requirements, especially small density variations, limit the applicability of conventional LB models for practical problems involving flow through porous media, because in these problems, fluid motion is often driven by large pressure gradients, or, equivalently, elevated density gradients. For low permeability media, even if the pore velocity (Mach number) is small, the pressure (density) gradient can be very large. Therefore, use of the conventional LB model to simulate flow in porous media may introduce significant density changes (and hence compressibility error). Furthermore, when the velocity field obtained from the conventional LB model is applied to solute transport simulation, one may obtain an unphysical breakthrough curve (breakthrough too early) for a tracer, or worse, an

unphysical disequilibrium of an otherwise chemically equilibrated system for reactive solutes [34]. This has been largely neglected in previous LB modeling of reacting flows.

Therefore, when flow and transport in porous media are concerned, an incompressible LB model is more desirable. There are several incompressible LB models in the literature. Here we only give a brief overview of the one constructed by Guo et al. [13] as it is applicable to both steady and unsteady flows. In this model, the evolution equation is the same as the conventional LBGK equation (2.1), but the equilibrium distribution equation is given by

$$f_\alpha^{\rm eq} = \begin{cases} -4\sigma\dfrac{p}{\rho c^2} + s_\alpha(\mathbf{u}), & \alpha = 0, \\ \lambda\dfrac{p}{\rho c^2} + s_\alpha(\mathbf{u}), & \alpha = 1-4, \\ \gamma\dfrac{p}{\rho c^2} + s_\alpha(\mathbf{u}), & \alpha = 5-8, \end{cases} \tag{2.6}$$

where σ, λ and γ are parameters satisfying

$$\lambda + \gamma = \sigma, \quad \lambda + 2\gamma = \frac{1}{2}.$$

Eq. (2.6) has been shown to recover the following incompressible NS equations [13]

$$\nabla \cdot \mathbf{u} = 0, \tag{2.7a}$$

$$\frac{\partial \mathbf{u}}{\partial t} + \nabla \cdot (\mathbf{u}\mathbf{u}) = -\frac{1}{\rho}\nabla p + \nu \nabla^2 \mathbf{u}, \tag{2.7b}$$

with the velocity and pressure given by

$$\mathbf{u} = \sum_{\alpha=1}^{8} \mathbf{e}_\alpha f_\alpha, \tag{2.8a}$$

$$\frac{p}{\rho} = \frac{c^2}{4\sigma}\Big(\sum_{\alpha=1}^{8} f_\alpha + s_0(\mathbf{u})\Big), \tag{2.8b}$$

and the viscosity is determined by

$$\nu = \frac{(\tau - \frac{1}{2})(\delta x)^2}{3\delta t}. \tag{2.9}$$

To demonstrate the compressibility effect of the conventional LB model on solute transport in porous media, we simulated flow and solute transport in a limestone rock at the pore scale. The pore structure was derived from a digitized image of a limestone rock thin section (Fig. 2). The size of the image is 320×240 lattice spacings, corresponding to a physical domain of 4×3 centimeters. Flow is simulated using the

Figure 2: Illustration of a rock thin section used in the flow and solute transport simulations. Black regions refer to solid grains.

conventional (compressible) and incompressible LB models. Solute transport is simulated using the LB model based on the two calculated velocity fields, i.e., compressible and incompressible velocity fields. The breakthrough curves for solute transport are compared with 1D FLOTRAN (a continuum scale model) simulations [33].

In Fig. 3 are shown breakthrough curves obtained with the 1D FLOTRAN simulation and with the LB simulations based on the compressible and incompressible velocity fields for two different pressure gradients. In the FLOTRAN simulation, the number of nodes is 320. The average Darcy velocity is calculated from the velocity field obtained using the incompressible LB model, the tortuosity is derived from separate simulations of diffusion through this porous medium using both LB and FLOTRAN simulations and the dispersivity remains a fitting parameter [34]. In the continuum-scale simulation using FLOTRAN, each node is assigned the same porosity, permeability, tortuosity, Darcy velocity and dispersivity values. Therefore, the medium used in the continuum-scale simulation is homogenized, with each node having the same medium properties of the whole medium, as it was treated in [24]. For the case of smaller pressure gradient, the three breakthrough curves coincide with each other

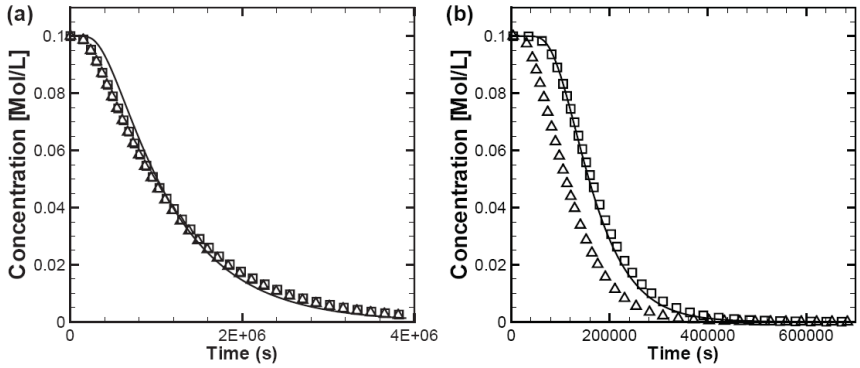

Figure 3: Time evolution of the concentration at the exit (breakthrough curve) for the thin section shown in Fig. 2. Solid line, square and diamond symbols denote the results of 1D FLOTRAN and LB simulations based on incompressible and compressible velocity fields, respectively. LB concentrations are averaged vertically: (a) Δp=0.02; (b) Δp=0.2, both in LB units.

(Fig. 3a), indicating that a single-continuum model with a homogenized medium is sufficient to simulate the transport process in the medium represented by the thin section, as far as the breakthrough curve is concerned. This conclusion is supported by the observation that most of the pore space in the medium is connected and accessible by flow, unlike the structured medium in [34], which has a significant amount of dead-end pore space only accessible by diffusion and hence has to be modeled by a dual-continuum model. For a larger pressure gradient, however, the breakthrough curve based on the compressible velocity field deviates from the other two curves by predicting an earlier breakthrough, as shown in Fig. 3b.

3 Lattice Boltzmann method for chemical reactions in the pore space

3.1 Kinetic reactions

The LB models for chemically reacting fluid flows were first introduced by [9, 29]. In their models, the LB equations for transport have a similar form as the flow equation with the addition of a source/sink term representing chemical reactions. The chemical reactions used in [9] represent the Selkov model. In a more general case, homogeneous chemical reactions taking place in an aqueous fluid can be written in the following form [21]:

$$0 \rightleftharpoons \sum_{k=1}^{N} \nu_{kr} A_k, \quad r = 1, \cdots, N_R, \tag{3.1}$$

where N is the total number of solute species, N_R is the number of reactions, A_k denotes the kth species and ν_{kr} is the stoichiometric coefficient. If the concentrations of the aqueous species are assumed to be sufficiently low so that their effect on the density and velocity of the solution is negligible, then the reactive transport of solute species can be described using another set of distribution functions, $g_{\alpha k}$, which satisfies a similar evolution equation as f_i

$$\begin{aligned} g_{\alpha k}(\mathbf{x} + \mathbf{e}_\alpha \delta t, t + \delta t) =& g_{\alpha k}(\mathbf{x}, t) - \frac{g_{\alpha k}(\mathbf{x}, t) - g^{\mathrm{eq}}_{\alpha k}(C_k, \mathbf{u})}{\tau_k} \\ &+ \omega_\alpha \sum_{r=1}^{N_R} \nu_{kr} I_r, \quad k = 1, \cdots, N, \end{aligned} \tag{3.2}$$

where I_r is the reaction rate of the r-th reaction, C_k is the solute concentration of the k-th species, τ_k is the relaxation time related to the diffusivity by

$$D_k = \frac{(\tau_k - 1/2)(\delta x)^2}{3\delta t}, \tag{3.3}$$

for the D2Q9 lattice, and $g^{\mathrm{eq}}_{\alpha k}$ is the equilibrium distribution function of the kth species, which has the following form:

$$g^{\mathrm{eq}}_{\alpha k}(C_k, \mathbf{u}) = \omega_\alpha C_k + C_k s_\alpha(\mathbf{u}), \tag{3.4}$$

the concentration C_k is defined in terms of the distribution function by the following equation

$$C_k = \sum_{\alpha} g_{\alpha k}, \tag{3.5}$$

similar to the density in the flow equation. Using the Chapman-Enskog expansion technique, one can prove that the above LB equation (3.2), recovers the pore-scale advection-diffusion-reaction equation for an incompressible flow field [9]

$$\frac{\partial C_k}{\partial t} + (\mathbf{u} \cdot \nabla) C_k = \nabla \cdot (D_k \nabla C_k) + \sum_{r=1}^{N_R} \nu_{kr} I_r. \tag{3.6}$$

Therefore, one can solve the reactive transport problem by solving Eq. (3.2) for each species, assuming all reaction rate constants are known.

Using their LB model, Dawson et al. [9] simulated pure diffusion, homogeneous chemical reactions and pattern formation due to Turing instability. Their numerical results agreed well with theoretical predictions and captured the basic physics as predicted by the macroscopic reaction-diffusion equations. Qian et al. [42] simulated front dynamics and scaling properties for the irreversible reaction: $A + B \rightarrow C$. They verified the asymptotic results concerning the scaling exponents and the scaling function of the production rate at long times. Weimar and Boon [52] simulated an athermal flow which advects reactant species. They considered a nonlinear reactive system described by the Brusselator model. Yan and Yuan [55] simulated the Belousov-Zhabotinskii reaction and showed that the LBM could capture the well-known chemical clock of the diffusion-reaction system. The reactive LBM has also been used to simulate combustion [11, 54], bacterial chemotaxis [16] and bacterial growth in porous media [56].

3.2 Local-equilibrium reactions

For a chemical system with many species, solving Eq. (3.2) for each species may be very computationally expensive. Moreover, to solve these equations would require knowledge of all the reaction rates I_r as functions of the species concentrations through kinetic rate laws. For many reactions, however, their intrinsic rates are sufficiently rapid that the reactions may be assumed to be in instantaneous equilibrium. Their actual rates are then controlled by the rate of transport of species to and from the site of reaction. For these reactions it would be desirable if the conservation equations could be formulated in such a way that rates corresponding to these fast reactions could be replaced by conditions of local equilibrium in the form of appropriate mass action equations.

In a previous paper, Kang et al. [21] have derived the following LB equation for the total primary species concentrations for chemical systems with reactions written in canonical form

$$G_{\alpha j}(\mathbf{x} + \mathbf{e}_\alpha \delta t, t + \delta t) = G_{\alpha j}(\mathbf{x}, t) - \frac{G_{\alpha j}(\mathbf{x}, t) - G^{\mathrm{eq}}_{\alpha j}(\Psi_j, \mathbf{u})}{\tau_{\mathrm{aq}}}, \tag{3.7}$$

where $j = 1, \cdots, N_C$, and N_C is the number of primary species, Ψ_j is the total concentration of the j-th primary species, $G_{\alpha j}$ is its distribution function along the α direction, $G^{\rm eq}_{\alpha j}$ is the corresponding equilibrium distribution function and $\tau_{\rm aq}$ is the dimensionless relaxation time for all the aqueous species. Here only species-independent diffusion is considered, guaranteeing conservation of charge in the aqueous phase. Different diffusion coefficients can be obtained by varying δx or δt in Eq. (3.3). More information on LBM simulation of electrochemical systems that includes species-dependent diffusion can be found in [15]. For the D2Q4 model, the equilibrium distribution takes the following linear form:

$$G^{\rm eq}_{\alpha j} = \frac{\Psi_j}{4} + \frac{\Psi_j}{2c^2}(\mathbf{e}_\alpha \cdot \mathbf{u}), \tag{3.8a}$$

with
$$\mathbf{e}_\alpha = \Big(\cos\frac{(\alpha-1)\pi}{2}, \sin\frac{(\alpha-1)\pi}{2}\Big)c, \quad \alpha = 1,2,3,4. \tag{3.8b}$$

Noble [39] has shown that Eq. (3.7) can recover the following pore-scale advection-diffusion equation for Ψ_j

$$\frac{\partial \Psi_j}{\partial t} + \nabla \cdot \mathbf{\Omega}_j = 0, \tag{3.9a}$$

with

$$\Psi_j = \sum_\alpha G_{\alpha j}, \tag{3.9b}$$

and
$$\mathbf{\Omega}_j = \mathbf{u}\Psi_j - \mathcal{D}\nabla\Psi_j, \tag{3.9c}$$

as the flux of the total concentration of the j-th primary species due to both advection and diffusion. The diffusivity is given by

$$\mathcal{D} = \frac{(\tau_{\rm aq} - 1/2)(\delta x)^2}{2\delta t}. \tag{3.10}$$

Assuming the homogeneous reactions are in instantaneous equilibrium, we have the following mass action equations [35,36]

$$C_i = (\gamma_i)^{-1} K_i \prod_{j=1}^{N_C} (\gamma_j C_j)^{\nu_{ji}}, \tag{3.11}$$

where ν_{ji} are the stoichiometric coefficients, K_i is the equilibrium constant of the i-th homogeneous reaction, γ_i is the activity coefficient of the i-th secondary species and C_j and C_i are solute concentrations for primary and secondary species, respectively. They are related to Ψ_j by

$$\Psi_j = C_j + \sum_{i=1}^{N_R} \nu_{ji} C_i, \tag{3.12}$$

where N_R is the number of independent homogeneous reactions, or, equivalently, secondary species.

Therefore, by rewriting the homogeneous reactions in the canonical form, formulating a LB equation for total concentration Ψ_j and replacing the rates of these reactions with mass action equations, the number of unknowns and evolution equations is re-

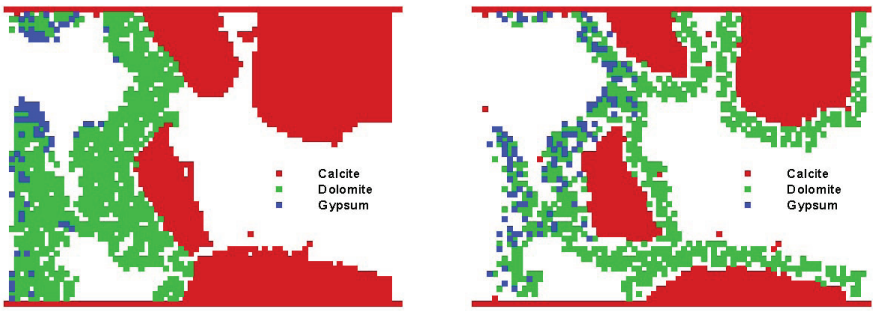

(a) (b)

Figure 4: Resulting geometries at time=15625 seconds for two different mineral reaction rate constants: (a) large reaction rate constants; (b) small reaction rate constants.

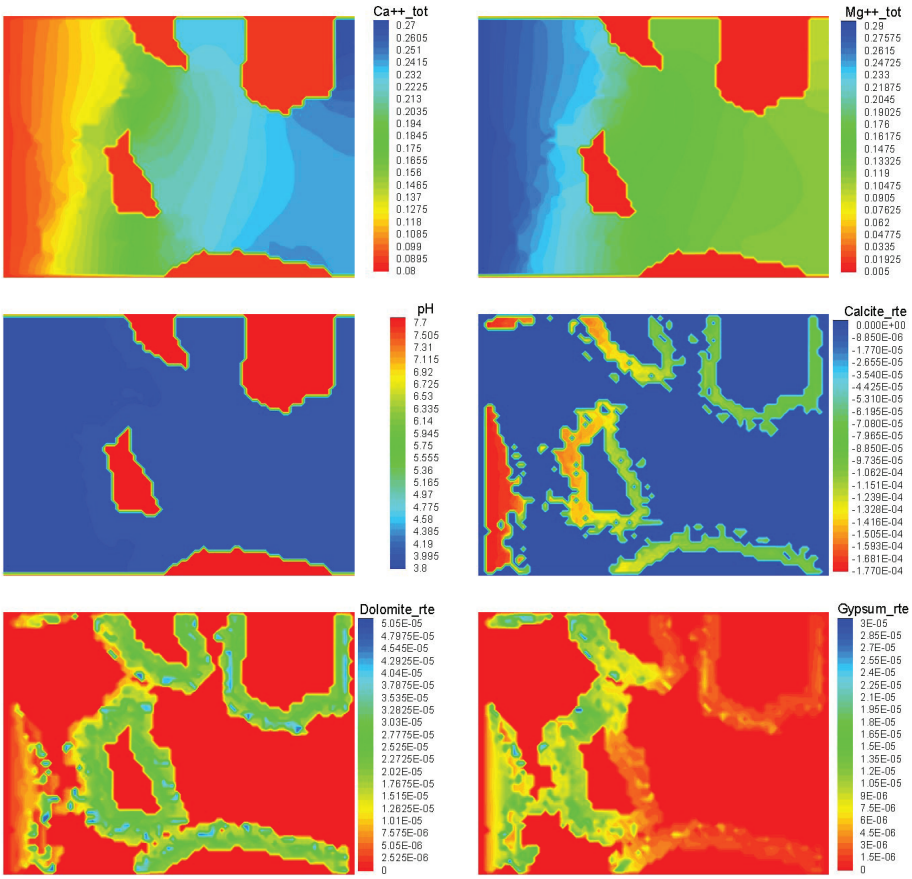

Figure 5: Distribution of solute concentrations, pH value and reaction rates at time=15625 seconds for small reaction rate constants.

duced from $N_C + N_R$ to N_C. The reduction can be significant for a system with many aqueous species, as demonstrated in the following example.

Kang et al. [19] simulated the injection of a fluid saturated with 170 bars CO_2(g) into a limestone rock at the pore scale. In their study, the pore structure shown in Fig. 2 is used. The chemical system of Na^+, Ca^{2+}, Mg^{2+}, H^+, SO_4^{2-}, CO_2(aq) and Cl^- with the reaction of calcite to form dolomite and gypsum is considered. Secondary species included in the simulation are: OH^-, HSO_4^-, H_2SO_4(aq), CO_3^{2-}, HCO_3^-, $CaCO_3$(aq), $CaHCO_3^+$, $CaOH^+$, $CaSO_4$(aq), $MgCO_3$(aq), $MgHCO_3^+$, $MgSO_4$(aq), $MgOH^+$, NaCl(aq), $NaHCO_3^-$(aq) and NaOH(aq). For this system, N_C=7, but $N_C + N_R$=23. Initial fluid composition is pH 7.75 and 2.69 m NaCl brine, equilibrium with minerals calcite, dolomite and gypsum at 25°C. Initial rock composition is calcite. Secondary minerals include dolomite and gypsum. For boundary conditions, a constant pressure gradient is imposed across the domain for flow. When flow reaches steady state, a fluid with a pH of 3.87 and in equilibrium with 179 bars CO_2(g) and minerals dolomite and gypsum is introduced at the inlet. Zero gradient boundary conditions are imposed at the outlet. Two different cases are considered with different mineral reaction rates to show their effects on solution concentration, mineral deposition and change in geometry. Resulting geometries at time=15625 seconds for two different mineral reaction rate constants are plotted in Fig. 4. Damkohler number is 7.375 for calcite and gypsum and 0.7375 for dolomite for the faster mineral reactions and 7.375×10^{-2} for calcite and gypsum and 7.375×10^{-3} for dolomite for slower reactions. Concentration distribution of total Ca^{2+} and Mg^{2+}, pH and reaction rates for calcite, dolomite and gypsum for the slower reactions are plotted in Fig. 5. The methods used to handle mineral reactions and to update solid phase will be discussed in the following sections.

As can been seen from the figures, as the reaction rate constants decrease, the deposition of dolomite becomes more uniform surrounding the dissolving calcite grains. Only a small amount of gypsum forms on top of dolomite. At some point in the simulation, the major pores for flow become blocked halting further fluid flow through the medium. The pH is uniform over the entire pore space. All reaction rates have finite values at the mineral surface in the whole domain, outlining the solid geometry. The reaction rate is negative for calcite and positive for dolomite and gypsum, confirming that calcite is dissolving while dolomite and gypsum are precipitating.

4 Lattice Boltzmann method for chemical reactions at fluid-solid interfaces

Early work on chemical reactions at solid surfaces was based on lattice gas automa (LGA). Wells et al. [53] pioneered an LGA model that coupled solute transport with chemical reactions at mineral surfaces and in pore networks. In their model, chemical reactions considered at solid surfaces included precipitation/dissolution, sorption and catalytic reaction. Dissolution and precipitation reactions were simulated by al-

lowing wall nodes to serve as sources or sinks for mass of a dissolved component. Whenever a particle collides with a wall, a unit of mass may be exchanged, thus increasing or decreasing the local concentration in solution depending upon the saturation state of the fluid.

Sullivan et al. [45,46] simulated 2D and 3D packed bed reactors using a LBM. They accounted for the local fluid velocity by including reaction via concentration changes in the equilibrium distribution. Miller et al. [38] simulated anisotropic crystal growth from melt, using a LBM with enhanced collisions for hydrodynamics coupled with a phase-field model for the anisotropic liquid/solid phase transition. Other LBMs treated chemical reactions at the fluid-solid interfaces through boundary conditions. Kelemen and co-workers [28] extended the LBM with a dissolution boundary condition such that the fluid particle colliding with the wall has a probability of detaching a solid particle. Verhaeghe and co-workers [49] designed boundary conditions to impose a concentration or a flux on a solid interface for use in multicomponent LBMs. Kang et al. [25–27] developed LB models for simulating coupled flow and dissolution/precipitation in porous media for systems with one or two aqueous species and simple reaction kinetics. In [27], they studied the effects of Peclet and Damköhler numbers on solid alteration and solute concentration and investigated the conditions at which the effects of dissolution and precipitation on solid alteration can be reversed approximately and minimize hysteresis. Later, Kang et al. [21] developed a more general LB pore-scale model for simulating reactive transport in systems with multiple aqueous components and minerals. Their model takes into account advection, diffusion, homogeneous reactions among multiple aqueous species, heterogeneous reactions between the aqueous solution and minerals, as well as the resulting geometrical changes in pore space.

In the models by Kang et al. [21,25–27], the boundary condition for the thermal LB model proposed by He et al. [14] was used to derive the boundary condition for the concentration distribution function at the fluid/solid interface. As a result, the solute mass is not strictly conserved by heterogeneous reactions occurring at the mineral interface. In a more recent publication, Kang and co-workers [22] rigorously derived the boundary condition for the distribution function of the total concentrations by using a correct expression of the particle distribution functions in terms of the corresponding total concentrations and their gradients and by using a relation satisfied by the non-equilibrium portion of the distribution functions. With this new boundary condition, the solute mass is strictly conserved.

In Kang et al.'s method, the following boundary condition for the total concentrations Ψ_j has been employed [21]

$$\mathcal{D}\frac{\partial \Psi_j}{\partial n} = -\sum_{m=1}^{N_m} \nu_{jm} k_m \left(1 - K_m Q_m\right). \tag{4.1}$$

In this equation, n is the direction normal to the interface pointing toward the fluid phase, k_m is the reaction rate constant, K_m is the equilibrium constant and the ion

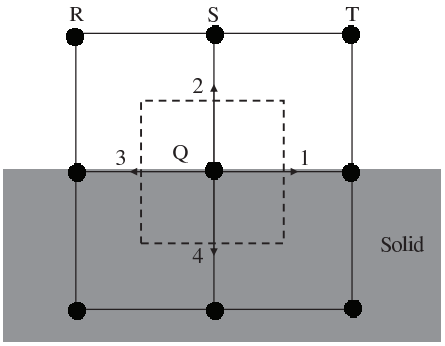

Figure 6: Schematic illustration of a D2Q4 lattice at a wall node.

activity product Q_m is defined by

$$Q_m = \prod_{j=1}^{N_C} (\gamma_j C_j)^{\nu_{jm}}. \tag{4.2}$$

The formulation of the unknown distribution functions at the fluid/solid interface depends on the orientation of the surface. For a wall node shown in Fig. 6, the unknown distribution function G_{2j} can be calculated by [22]

$$G_{2j} = \frac{\Psi_j}{2} - G_{4j}, \tag{4.3}$$

where Ψ_j is determined from Eq. (3.12) after C_j is calculated from the following nonlinear algebraic equation through the Newton-Raphson iteration method

$$2G_{4j} = \frac{\Psi_j}{2} - \frac{1}{c} \sum_{m=1}^{N_m} \nu_{jm} k_m (1 - K_m Q_m). \tag{4.4}$$

5 Update of solid phase

To accurately model chemical reactions at fluid-solid interfaces, it is necessary to account for the time evolution of solid phase, especially when significant mass transfer between solids and fluids is involved due to dissolution and/or precipitation. Verberg and Ladd [47, 48] designed an algorithm for simulation of chemical erosion in rough fractures. An optimized LB scheme is used to solve the time-independent Stokes flow equations. A continuous bounce-back scheme allows for the boundary to be located anywhere between two grid nodes. The new solid structure is determined based on the local flux of tracer particles across the solid surface, where the assumption is made that the reaction kinetics are instantaneous and that the dissolution is therefore diffusion controlled. In Verhaeghe's work, the amount of species injected in the system was calculated from the difference between populations leaving and entering the system.

The amount of dissolved solid was then made equal to the amount of injected species divided by the difference between the solid concentration and the actual concentration in the cell. Kang et al. [20] proposed two methods to update solid phase. In both methods, the volume of the stationary solids satisfies the following equation

$$\frac{\partial V_m}{\partial t} = \overline{V}_m a_m I_m^*, \tag{5.1}$$

where V_m, $\overline{V}_m$ and a_m are dimensionless volume, molar volume and specific surface area of the m-th mineral, respectively and I_m^* is the reaction rate for the m-th mineral reaction at the mineral interface. Solute diffusion in the solid phase is neglected and mineral reactions are assumed to only occur at the fluid-solid interface. Each interface node represents a control volume (a control area in the 2D case) with a size of 1×1 (in lattice units) and is located at the center of this volume. As can be seen from Fig. 6, node Q is the center of the control volume surrounded by dashed lines. The initial control volume is given a dimensionless volume V_m^0. The volume is updated at each time step explicitly according to the equation

$$V_m(t + \delta t) = V_m(t) + \overline{V}_m a_m I_m^* \delta t, \tag{5.2}$$

where δt is the time increment. In this study both δt and a_m equal unity in lattice units.

When V_m reaches certain threshold values, the pore geometry needs to be updated. For dissolution, the solid node associated with V_m can be simply removed (i.e., changed to a pore node), when V_m reaches zero. For precipitation, however, there are multiple ways to add a solid node when V_m reaches a certain threshold value. A random-growth method was proposed by Kang et al. for both single-species [25, 27] and multi-component systems [21]. In that method, the growth has no preference in any particular direction and the method has been shown to be lattice-effect free. Fig. 7 shows crystal growth from a supersaturated solution of a single species based on this random-growth method. Clearly crystal shape in case (d) is a fairly round shape. Growth in preferred directions can be achieved by incorporating corresponding physics in the growth rules. For example, polygonal and dendritic crystals with symmetry have been produced by aligning the direction of growth to that of the maximum concentration gradient and different morphologies have been obtained by varying the probability of adding a solid node in that direction [37]. The results shown in Fig. 4 are also based on the random-growth method, but for a multi-component system.

In the above methods, the grid size is assumed to be small enough that each node is only represented by one mineral at one time and the effect of both dissolution and precipitation is recorded at that node through Eq. (5.2). In reality, changes of solid morphology can involve scales much smaller than the lattice or pore size used in the simulations. In another method, we assume that each node can be represented by multiple minerals whose initial total volume fraction amounts to unity. The volume fraction of each mineral is still updated by Eq. (5.2) and dissolution recorded in

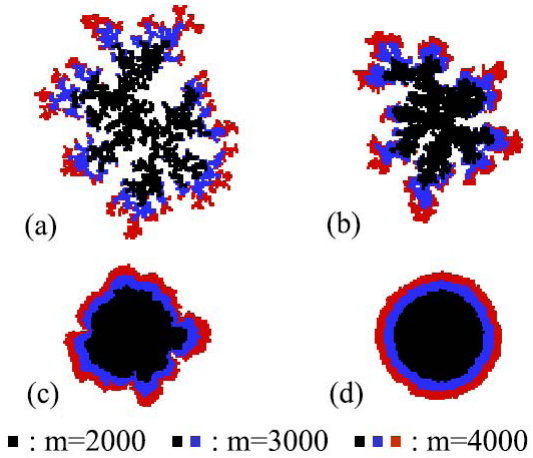

Figure 7: Crystal structures developed at different *Da* numbers and at solute saturation 1.2: (a) *Da*=600; (b) *Da*=150; (c) *Da*=48; (d) *Da*=2.

the solid node. Mass accumulation due to precipitation, however, is recorded at the neighboring pore nodes. As seen in Fig. 6, when

$$\sum_m V_m(Q) = 0, \tag{5.3}$$

node Q is changed to a fluid node. When

$$\sum_m V_m(S) = 1, \tag{5.4}$$

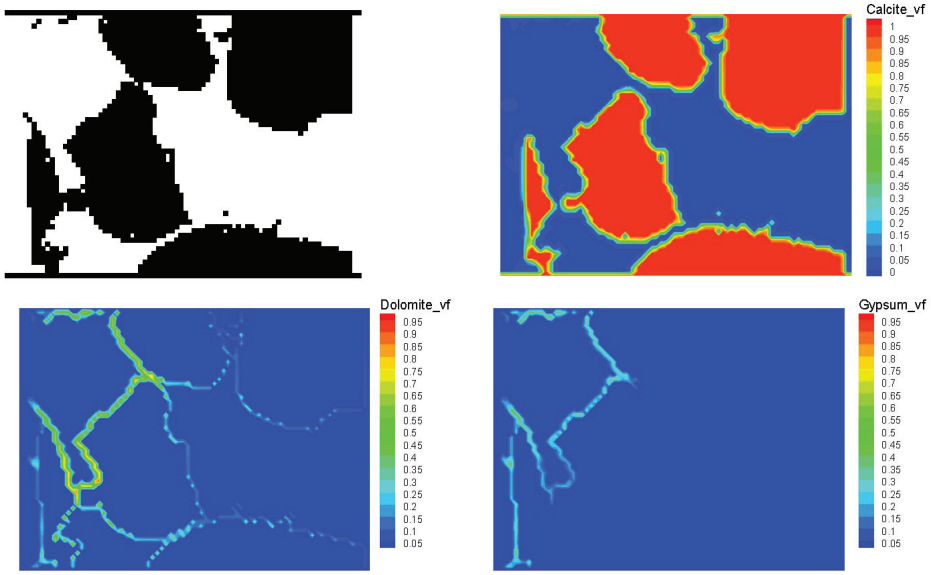

Figure 8: Resulting geometry (black and white) and volume fraction for the smaller reaction rate constants.

node S becomes a solid node composed of multiple minerals. In contrast to previous methods [21, 27] for updating pore geometry, the current method can account for coexistence of multiple minerals at the same node and the growth is deterministic rather than random. Fig. 8 shows resulting geometry and volume fraction for the smaller reaction rate constants using this method to update the solid phase. Now some solid nodes are not pure, but consist of different minerals. Their composition can be seen from the volume fraction of each mineral. Although the methods used are totally different, there is a strong resemblance between Figs. 4 (b) and 8 regarding the final porous medium structure and distribution of different minerals.

Clearly, the LBM can be used to simulate a variety of reacting flow problems when combined with appropriate methods to update the solid phase that account for the underlying physical properties/processes. Knutson et al. [30] simulated biofilm growth in porous media using the combined LBM, a final volume method and a cellular automata algorithm. Schulenburg et al. [50] presented the first numerical 3D pore-scale model of biofilm growth in porous media, based on an LB simulation platform complemented with an individual-based biofilm model (IbM). Pintelon et al. [40] also simulated biofilm growth using an LB simulation platform complemented with the IbM. In addition, in their method, a biomass detachment technique was included using a fast marching level set (FMLS) method that modeled the propagation of the biofilm-liquid interface with a speed proportional to the adjacent velocity shear field.

6 Future applications

We envision that continuous progress in the area of reacting flows in complex media can be made in the near future, which will enable the LBM to be applied to more challenging problems.

Seafloor hydrothermal system vents are a good example. As highly dynamic systems involving transfer of high temperature solutions from the crust across the seafloor interface, they offer a complex environment where chemical reactions, fluid flow and detailed physical structures must be modeled. They are also potential "gold mines" of metals and unique biological materials such as metal-tolerant and chemosynthetic bacteria that are of major economic importance [18]. These systems have coupled physical, chemical and biological processes, to which the LBM is well suited. In addition to flow and chemical reactions in complex geometries, to simulate the processes and growth of chimney structures at seafloor hydrothermal vents, the moving particle capability [1, 7, 31, 32] should be incorporated into the multi-component reactive LBM.

The chemical reactions presented so far are all non-electrochemical reactions. Another important development of the LBM is to enable it to account for electrochemical reactions. Electrochemical processes occur in natural systems as well as in industrial processes, including treatment of acid mine drainage, oxidation of organic pollutants, nuclear waste disposal and many others. He and Li [15] proposed a multiple LBM

procedure for the electrochemical systems, but they used a local neutrality law to constrain the electric potential distribution, which could be inaccurate for charged mineral surfaces. Recently, Wang and Kang [51] developed a numerical framework to solve the dynamic model for electrokinetic flow using coupled LBM. Work on incorporating this numerical framework with the multi-component reactive LBM is ongoing.

One particular interesting electrochemical process is localized corrosion. Localized corrosion and prediction of scale structure and properties are at the cutting-edge of research in corrosion science [57]. Applications range from nuclear power and waste to beryllium alloys to weapons to oil pipelines. Modeling a galvanic mechanism that facilitates the localized corrosion requires charge separation between the anode and cathode that cannot be represented in continuum reactive transport models but is well suited to LBM. Again, the current LBM models for reactive transport need to be augmented to calculate local chemical and electrochemical potentials [51] to predict rates of reactions and the development/deterioration of scales.

7 Conclusions

We have reviewed recent progress on the lattice Boltzmann simulation of reacting flows in porous media. We want to emphasize the flexibility and ease of this method in handling coupled flow and multiple physicochemical processes in complex media. We are fully aware that this is an interdisciplinary area undergoing rapid development and hence it is not possible to include all interesting applications or new developments. We are hoping that this article can provide some useful information for those who are interested in this topic.

Acknowledgments

This work was supported by LDRD project 20100025DR sponsored by Los Alamos National Laboratory and by UC Lab Fees Research Project UCD-09-15.

References

[1] C. K. AIDUN AND Y. N. LU, *Lattice boltzmann simulation of solid particles suspended in fluid*, Journal of Statistical Physics, 81(1-2) (1995), pp. 49–61.

[2] S. BEKRI, J. F. THOVERT AND P. M. ADLER, *Dissolution of porous media*, Chemical Engineering Science, 50(17) (1995), pp. 2765–2791.

[3] S. BEKRI, J. F. THOVERT AND P. M. ADLER, *Dissolution and deposition in fractures*, Engineering Geology, 48(3-4) (1997), pp. 283–308.

[4] HUDONG CHEN, SHIYI CHEN AND WILLIAM H. MATTHAEUS, *Recovery of the navier-stokes equations using a lattice-gas boltzmann method*, Physical Review A, 45(8) (1992), R5339.

[5] S. CHEN, S. P. DAWSON, G. D. DOOLEN, D. R. JANECKY AND A. LAWNICZAK, *Lattice methods and their applications to reacting systems*, Computers & Chemical Engineering, 19(6-7) (1995), pp. 617–646.
[6] S. CHEN AND G. D. DOOLEN, *Lattice boltzmann method for fluid flows*, Annual Review of Fluid Mechanics, 30 (1998), pp. 329–364.
[7] K. CONNINGTON, Q. J. KANG, H. VISWANATHAN, A. ABDEL-FATTAH AND S. Y. CHEN, *Peristaltic particle transport using the lattice boltzmann method*, Physics of Fluids, 21(5) (2009), 053301.
[8] G. DACCORD, *Chemical dissolution of a porous medium by a reactive fluid*, Physical Review Letters, 58(5) (1987), pp. 479–482.
[9] S. PONCE DAWSON, S. CHEN AND G. D. DOOLEN, *Lattice boltzmann computations for reaction-diffusion equations*, The Journal of Chemical Physics, 98(2) (1993), pp. 1514–1523.
[10] PETER DIJK AND BRIAN BERKOWITZ, *Precipitation and dissolution of reactive solutes in fractures*, Water Resour. Res., 34 (1998), pp. 457–470.
[11] O. FILIPPOVA AND D. HANEL, *Lattice-bgk model for low mach number combustion*, International Journal of Modern Physics C, 9(8) (1998), pp. 1439–1445.
[12] C. N. FREDD AND H. S. FOGLER, *Influence of transport and reaction on wormhole formation in porous media*, AIChE Journal, 44(9) (1998), pp. 1933–1949.
[13] Z. L. GUO, B. C. SHI AND N. C. WANG, *Lattice bgk model for incompressible navier-stokes equation*, Journal of Computational Physics, 165(1) (2000), pp. 288–306.
[14] X. HE, S. CHEN AND G. D. DOOLEN, *A novel thermal model for the lattice boltzmann method in incompressible limit*, Journal of Computational Physics, 146(1) (1998), pp. 282–300.
[15] XIAOYI HE AND NING LI, *Lattice boltzmann simulation of electrochemical systems*, Computer Physics Communications, 129(1-3) (2000), pp. 158–166.
[16] M. HILPERT, *Lattice-boltzmann model for bacterial chemotaxis*, Journal of Mathematical Biology, 51(3) (2005), pp. 302–332.
[17] M. L. HOEFNER AND H. S. FOGLER, *Pore evolution and channel formation during flow and reaction in porous media*, AIChE Journal, 34(1) (1988), pp. 45–54.
[18] D. R. JANECKY AND W. E. SEYFRIED, *Formation of massive sulfide deposits on oceanic ridge crests- incremental reaction models for mixing between hydrothermal solutions and seawater*, Geochimica Et Cosmochimica Acta, 48(12)(1984), pp. 2723–2738.
[19] Q. KANG, M. WANG, P. P. MUKHERJEE AND P. C. LICHTNER, *Mesoscopic modeling of multi-physicochemical transport phenomena in porous media*, Advances in Mechanical Engineering, 2010:doi:10.1155/2010/142879, 2010.
[20] Q. J. KANG, P. C. LICHTNER, H. S. VISWANATHAN AND A. I ABDEL-FATTAH, *Pore scale modeling of reactive transport involved in geologic co2 sequestration*, Transport in Porous Media, 82(1) (2010), pp. 197–213.
[21] Q. J. KANG, P. C. LICHTNER AND D. X. ZHANG, *Lattice boltzmann pore-scale model for multicomponent reactive transport in porous media*, J. Geophys. Res., 111(5) (2006), article ID B05203.
[22] Q. J. KANG, P. C. LICHTNER AND D. X. ZHANG, *An improved lattice boltzmann model for multicomponent reactive transport in porous media at the pore scale*, Water Resources Research, 43(12) (2007), article ID W12S15.
[23] Q. J. KANG, I. N. TSIMPANOGIANNIS, D. X. ZHANG AND P. C. LICHTNER, *Numerical modeling of pore-scale phenomena during co2 sequestration in oceanic sediments*, Fuel Processing Technology, 86(14-15) (2005), pp. 1647–1665.
[24] Q. J. KANG, D. X. ZHANG AND S. Y. CHEN, *Unified lattice boltzmann method for flow in multiscale porous media*, Physical Review E, 66 (2002), 056307.

[25] Q. J. KANG, D. X. ZHANG AND S. Y. CHEN, *Simulation of dissolution and precipitation in porous media*, Journal of Geophysical Research-Solid Earth, 108(B10) (2003), pp. 2505–2513.

[26] Q. J. KANG, D. X. ZHANG, S. Y. CHEN AND X. Y. HE, *Lattice boltzmann simulation of chemical dissolution in porous media*, Physical Review E, 65(3) (2002), 036318.

[27] Q. J. KANG, D. X. ZHANG, P. C. LICHTNER AND I. N. TSIMPANOGIANNIS, *Lattice boltzmann model for crystal growth from supersaturated solution*, Geophysical Research Letters, 31 (2004), pp. L21604.1–L21604.5.

[28] PETER B. KELEMEN, J. A. WHITEHEAD, EINAT AHARONOV AND KELSEY A. JORDAHL, *Experiments on flow focusing in soluble porous media, with applications to melt extraction from the mantle*, J. Geophys. Res., 100 (1995), pp. 475–496.

[29] R. D. KINGDON AND P. SCHOFIELD, *A reaction-flow lattice boltzmann model*, Journal of Physics a-Mathematical and General, 25(14) (1992), pp. L907–L910.

[30] C. E. KNUTSON, C. J. WERTH AND A. J. VALOCCHI, *Pore-scale simulation of biomass growth along the transverse mixing zone of a model two-dimensional porous medium*, Water Resources Research, 41(7) (2005), W07007.

[31] A. J. C. LADD, *Numerical simulations of particulate suspensions via a discretized boltzmann-equation .1. theoretical foundation*, Journal of Fluid Mechanics, 271 (1994), pp. 285–309.

[32] A. J. C. LADD, *Numerical simulations of particulate suspensions via a discretized boltzmann-equation .2. numerical results*, Journal of Fluid Mechanics, 271 (1994), pp. 311–339.

[33] P. C. LICHTNER, *Flotran user manual*, Technical report, Los Alamos National Laboratory, 2001.

[34] P. C. LICHTNER AND Q. KANG, *Upscaling pore-scale reactive transport equations using a multiscale continuum formulation*, Water Resources Research, 43(12) (2007), W12S15.

[35] P C LICHTNER, C I STEEFEL AND E H OELKERS, Reactive Transport in Porous Media, Volume 34 of Reviews in mineralogy, Mineralogical Society of America, Washington, D. C., 1996.

[36] PETER C. LICHTNER, *Continuum model for simultaneous chemical reactions and mass transport in hydrothermal systems*, GEOCHIMICA ET COSMOCHIMICA ACTA, 49(3):779–800, 1985. doi: DOI: 10.1016/0016-7037(85)90172-3.

[37] G. P. LU, D. J. DEPAOLO, Q. J. KANG AND D. X. ZHANG, *Lattice boltzmann simulation of snow crystal growth in clouds*, Journal of Geophysical Research-Atmospheres, 114 (2009), D07305.

[38] W. MILLER, S. SUCCI AND D. MANSUTTI, *Lattice boltzmann model for anisotropic liquid-solid phase transition*, Physical Review Letters, 86(16) (2001), pp. 3578–3581.

[39] D. R. NOBLE, Lattice Boltzmann Study of the Interstitial Hydrodynamics and Dispersion in Steady Intertial Flows in Large Randomly Packed Beds, PhD thesis, UIUC, 1997.

[40] T. R. R. PINTELON, D. A. G. VON DER SCHULENBURG AND M. L. JOHNS, *Towards optimum permeability reduction in porous media using biofilm growth simulations*, Biotechnology and Bioengineering, 103(4) (2009), pp. 767–779.

[41] Y. H. QIAN, D. DHUMIERES AND P. LALLEMAND, *Lattice bgk models for navier-stokes equation*, Europhysics Letters, 17(6BIS) (1992), pp. 479–484.

[42] Y. H. QIAN AND S. A. ORSZAG, *Scalings in diffusion-driven reaction a+b- c - numerical simulations by lattice bgk models*, Journal of Statistical Physics, 81(1-2) (1995), pp. 237–253.

[43] J. SALLES, J. F. THOVERT AND P. M. ADLER, *Deposition in porous media and clogging*, Chemical Engineering Science, 48(16) (1993), pp. 2839–2858. DOI: 10.1016/0009-2509(93)80031-K.

[44] S. SUCCI, The Lattice Boltzmann Equation for Fluid Dynamics and Beyond. Numerical

Mathematics and Scientific Computation, Oxford University Press, 2001.

[45] S. P. SULLIVAN, L. F. GLADDEN AND M. L. JOHNS, *3d chemical reactor lb simulations*, Mathematics and Computers in Simulation, 72(2-6) (2006), pp. 206–211. Sullivan, Simon P. Gladden, Lynn F. Johns, Michael L. 14th International Conference on Discrete Simulation of Fluid Dynamics in Comples Systems AUG 22-26, 2005 Kyoto, JAPAN.

[46] S. P. SULLIVAN, F. M. SANI, M. L. JOHNS AND L. F. GLADDEN, *Simulation of packed bed reactors using lattice boltzmann methods*, Chemical Engineering Science, 60(12) (2005), pp. 3405–3418.

[47] R. VERBERG AND A. J. C. LADD, *Lattice-boltzmann model with sub-grid-scale boundary conditions*, Physical Review Letters, 84(10) (2000), pp. 2148–2151.

[48] R. VERBERG AND A. J. C. LADD, *Simulation of chemical erosion in rough fractures*, Physical Review E, 65(5) (2002), 056311.

[49] F. VERHAEGHE, S. ARNOUT, B. BLANPAIN AND P. WOLLANTS, *Lattice-boltzmann modeling of dissolution phenomena*, Physical Review E, 73(3) (2006), 036316, Part 2.

[50] D. A. G. VON DER SCHULENBURG, T. R. R. PINTELON, C. PICIOREANU, M. C. M. VAN LOOSDRECHT AND M. L. JOHNS, *Three-dimensional simulations of biofilm growth in porous media*, Aiche Journal, 55(2) (2009), pp. 494–504.

[51] M. R. WANG AND Q. J. KANG, *Modeling electrokinetic flows in microchannels using coupled lattice boltzmann methods*, Journal of Computational Physics, 229(3) (2010), pp. 728–744.

[52] J. R. WEIMAR AND J. P. BOON, *Nonlinear reactions advected by a flow*, Physica A, 224(1-2) (1996), pp. 207–215. Conference on Dynamics of Complex Systems AUG 06-11, 1995 CALCUTTA, INDIA.

[53] J. T. WELLS, D. R. JANECKY AND B. J. TRAVIS, *A lattice gas automata model for heterogeneous chemical reactions at mineral surfaces and in pore networks*, Physica D: Nonlinear Phenomena, 47(1-2) (1991), pp. 115–123. DOI: 10.1016/0167-2789(91)90284-G.

[54] K. YAMAMOTO, X. Y. HE AND G. D. DOOLEN, *Simulation of combustion field with lattice boltzmann method*, Journal of Statistical Physics, 107(1-2) (2002), pp. 367–383. 9th Annual International Conference on Discrete Simulation of Fluid Dynamics AUG 21-24, 2000 SANTA FE, NEW MEXICO.

[55] G. W. YAN AND L. YUAN, *A lattice boltzmann method for the chemical clock in the belousov-zhabotinskii reaction*, Chinese Physics Letters, 18(7) (2001), pp. 918–920.

[56] C. Y. ZHANG, Q. J. KANG, X. WANG, J. L. ZILLES, R. H. MULLER AND C. J. WERTH, Effects of pore-scale heterogeneity and transverse mixing on bacterial growth in porous media. Environmental Science & Technology, 44(8) (2010), pp. 3085–3092.

[57] J. S. ZHANG, *A review of steel corrosion by liquid lead and lead-bismuth*, Corrosion Science, 51(6) (2009), pp. 1207–1227.